$CuAl_2$相对铜铝钎焊接头组织与性能的影响

张 满[1,2]，薛松柏[1]，姬 峰[1]，娄银斌[3]，王水庆[3]

（1. 南京航空航天大学 材料科学与技术学院，南京 210016；2. 淮阴工学院 机械工程学院，江苏 淮安 223001；
3. 浙江新锐焊接材料有限公司，浙江 嵊州 312000）

摘 要：采用 Zn-Al钎料和自制 $KAlF_4$-$CsAlF_4$钎剂配合火焰钎焊方法对紫铜和纯铝进行钎焊，研究了钎料中铝含量变化对钎料铺展性能、钎料组织及钎焊接头力学性能的影响. 结果表明，钎料中铝含量质量分数为 15%时，钎焊接头力学性能最佳. 采用光学显微镜和场发射扫描电子显微镜进一步观察分析钎料组织、铜铝钎焊接头区域显微组织和铜侧界面层化合物的分布形态，并采用 EDS进行成分分析. 当钎料中铝含量较低时，铜铝钎焊接头区域主要由锌基固溶体构成，随着铝含量的升高，钎缝内部出现硬脆的 $CuAl_2$相，当铝含量质量分数达到 22%时，$CuAl_2$相尺寸变得粗大且分布不均匀，钎焊接头强度降低.

关键词：铜铝接头；力学性能；显微组织；$CuAl_2$相

中图分类号：TG425 文献标识码：A 文章编号：0253－360X(2011)02－0093－04

张 满

0 序 言

铜铝两种有色金属因其优异的电导性、热导性以及良好的力学性能，已经广泛应用于电力、制冷和化工行业. 由于紫铜密度大且价格高，在适当的场合用纯铝代替紫铜被认为是降低成本的有效途径，因此铜铝异种金属接头便不可避免的出现在众多工业产品的制造过程中. 但紫铜和纯铝存在较大的物理和化学性能差异，如熔点、熔化潜热、线膨胀系数等，实现铜铝可靠焊接并形成合格的焊接接头存在较大困难. 特别是紫铜和纯铝之间有很高的化学亲和力，当温度超过 120 ℃时铜铝之间便会生成脆性的金属间化合物，从而降低铜铝接头的性能，并易导致接头热裂纹的出现[1－4].

目前在铜铝异种金属焊接的研究过程中，研究者往往倾向于使用固相连接方法. Abbas等人[4]用冷压焊方法对铜铝进行了连接，并研究了 Al/Cu界面金属间化合物的生长规律. Lee等人[5]对 Al/Cu摩擦焊接头的组织和性能进行了详细研究. 而 Ouyang等人[6]则尝试用搅拌摩擦焊的方法对紫铜和铝合金进行了焊接. 紫铜和纯铝之间的钎焊则多局限于锡基钎料软钎焊和 Al-Si钎料中温钎焊[7]，而这两种钎料都无法获得具有良好性能的铜铝接头. 文中采用 Zn-Al钎料对铜铝接头进行了钎焊，钎焊方法为设备简单且易普及推广的氧乙炔火焰钎焊，研究了不同铝含量的钎料组织和性能，并对铜铝钎焊接头显微组织和性能进行了详细说明.

收稿日期：2010－09－14
基金项目：科技部科技人员服务企业行动基金资助项目（2009GJC20040）

1 试验方法

试验用 Zn-Al钎料成分如表 1所示，钎剂采用自制 $KAlF_4$-$CsAlF_4$无腐蚀性钎剂. 钎焊试验用母材为工业纯铝和 T2紫铜. 纯铝和紫铜试样分别用 5% NaOH和 15% H_2SO_4进行焊前清洗.

表 1 试验用钎料化学成分（质量分数，%）

Table 1 Composition of Zn-Al filler metals

元素	1	2	3	4	5	6
Al	2	5	12	15	18	22
Zn	98	95	88	85	82	78

钎料铺展试验参照国家标准 GB/T11364—2008，铺展试验将 0.1 g钎料放于试件上，在 520 ℃±5 ℃的恒温电阻炉中保温 15 min. 钎焊方法为火焰钎焊，钎焊接头形式为搭接. 取 Zn-2Al，Zn-15Al和 Zn-22Al三种钎料用于纯铝和紫铜试样的钎焊，采用万能试样拉伸机测试接头强度. 铝含量对钎料组

织及铜铝钎焊接头显微组织的影响分别用光学显微镜和日立 S-4800场发射电子显微镜进行观察分析.

2 试验结果及分析

2.1 铝含量对 Zn-Al钎料铺展性能的影响

铺展性能试验结果见图 1. 随着铝含量的增加,钎料在铝板上的铺展面积呈现先增后减的趋势.

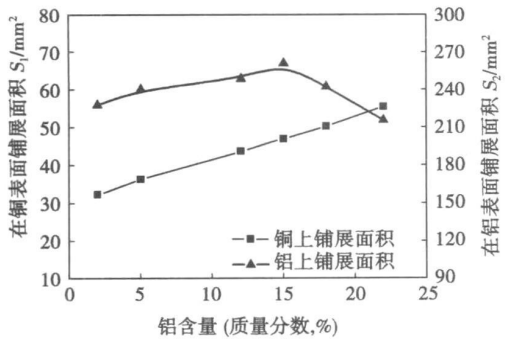

图 1 不同成分 Zn-Al钎料的铺展面积

Fig. 1 Spreading area of Zn-Al filler metals with different components

锌与铝互溶度很大,当锌基钎料在铝板上铺展时, Zn元素快速向铝基体中渗透致使锌基钎料在铝板上的润湿性变差. 增加钎料中的铝含量可以降低 Zn元素向铝板内的扩散速率,从而提高钎料在铝板上的铺展性能. 铝含量质量分数为 15%时,铺展面积达到最大,继续增加铝含量,由于钎料熔点升高导致的钎料熔体粘滞性增加作用变得显著,钎料流动性降低,铺展性能下降.

由图 1可知,随着铝含量的增加,钎料在铜板上铺展面积逐渐增大. 钎料与基体之间存在一定的相互作用有利于钎料的铺展. Al元素易与铜反应生成化合物,因此增加钎料中 Al元素的含量可以增加钎料在铜板上的铺展面积.

2.2 铝含量对钎料组织及钎焊接头强度的影响

钎料中铝含量的变化对钎料组织及钎焊接头力学性能影响较大. 图 2为 Zn-2Al, Zn-15Al和 Zn-22Al三种钎料熔化后缓冷的显微组织. 由锌铝相图可知 Zn-2Al属于亚共晶成分,钎料组织由块状初生相和 Zn-Al共晶组织构成,块状初生相应为锌基固溶体,块状组织周围黑白相间的为共晶组织,共晶组织由锌基固溶体与铝基固溶体混合构成. 当钎料中铝含量质量分数增加至 15%时,钎料成分处于过共晶区域,钎料中的块状组织应为由铝基固溶体初生相发生偏析反应生成的偏析组织,块状组织周围为共晶组织,如图 2b所示. Zn-22Al为偏析点,钎料组织全部由偏析组织构成.

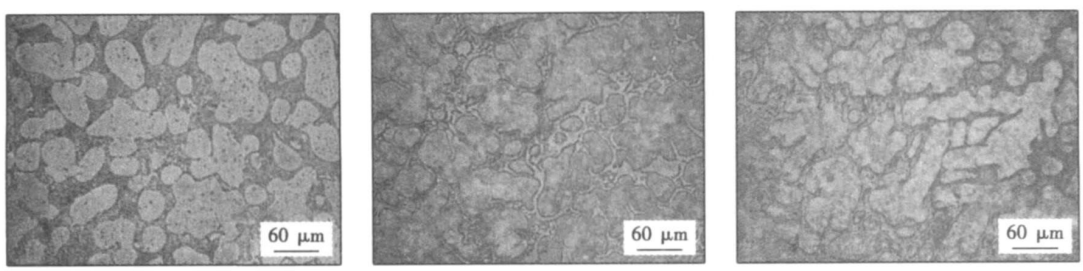

(a) Zn-2Al (b) Zn-15Al (c) Zn-22Al

图 2 钎料金相组织

Fig. 2 Optical micrographs of filler metals

由图 2可以看出,随着铝含量的增加,钎料的组织逐渐粗化,铝含量质量分数为 22%时,钎料的块状组织最为粗大.

上述三种钎料搭接钎焊接头抗剪强度如图 3所示. 试验结果表明试样均断裂于钎缝处, Zn-2Al和 Zn-22Al钎焊接头的抗剪强度相当,分别为 39.28 MPa和 39.22 MPa,而 Zn-15Al钎焊接头则较上述两种钎料钎焊接头强度高出 10.81%达到 44.04 MPa.

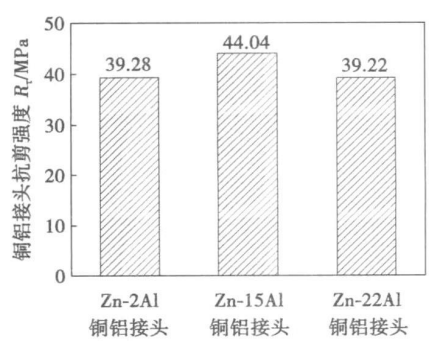

图 3 铜铝钎焊接头抗剪强度

Fig. 3 Shear strength of Cu/Al brazed joints

2.3 铝含量对铜铝钎焊接头显维组织的影响

Zn-2Al, Zn-15Al及 Zn-22Al铜铝钎缝显微组织见图 4. Zn-2Al铜铝钎焊钎缝显微组织主要为分布均匀的锌基固溶体,辅以少量的 Zn-Al共晶组织和 α-Al固溶体,钎缝中并无块状化合物出现. 当钎料中铝含量质量分数增加至 15%时,钎缝内出现大量化合物颗粒,通过 EDS分析并对照 Cu-Al二元相图可知该相为 $CuAl_2$相,均匀分布的 $CuAl_2$相可以起到颗粒强化的作用,有利于提高接头强度. 铝含量质量分数增加至 22%时,块状的 $CuAl_2$相 (图 4c,表 2)尺寸变得粗大且分布不均匀,在外力作用下,粗大的 $CuAl_2$相与周围组织界面处容易产生应力集

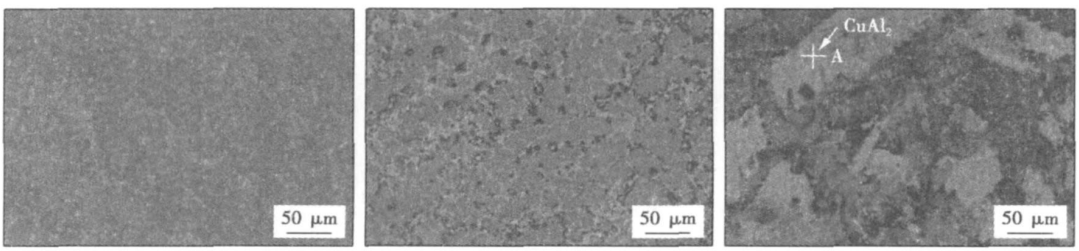

(a) Zn-2Al　(b) Zn-15Al　(c) Zn-22Al

图 4　Cu/Al钎焊缝显微组织

Fig. 4　SEM micrographs of Cu/Al brazing seam

表 2　A点能谱分析结果 (原子分数, %)

Table 2　EDS analysis results of spot A

位置	Al	Cu	Zn
A	63.46	34.58	1.96

中,导致裂纹萌生,钎焊接头强度降低.

钎缝铜侧界面层显微组织见图 5. Zn-15Al钎焊接头界面处化合物呈锯齿状,将钎缝与基体牢牢地“钉扎”在一起,能够阻止裂纹的扩展从而提高接头的强度,同时界面附近细小的 $CuAl_2$相 (图 5b,表 3)可以起到颗粒强化的作用. 而 Zn-22Al钎焊接头铜侧界面处的化合物多为粗大的条状,这是由于 Zn-22Al钎料熔点较高,钎焊加热时间较长,钎料与铜的反应较为剧烈,形成的化合物不仅较厚而且会生长的更大. 在外力作用下,粗大的条状化合物与周围组织容易产生应力集中而萌生裂纹,导致接头强度降低,界面附近粗大的 $CuAl_2$相 (图 5c,表 3)亦容易导致应力集中,使接头强度降低.

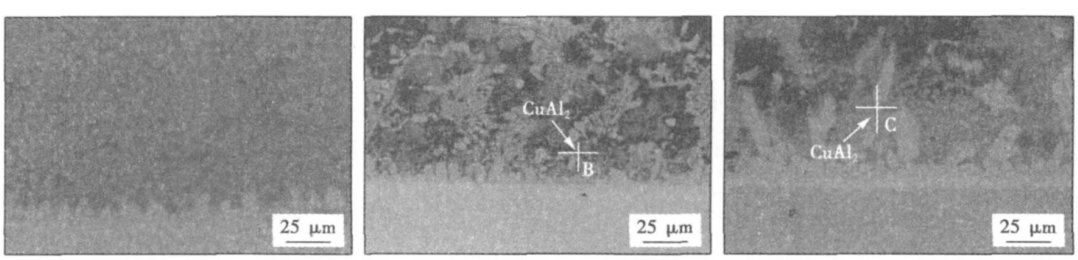

(a) Zn-2Al　(b) Zn-15Al　(c) Zn-22Al

图 5　铜侧界面化合物分布形态

Fig. 5　SEM micrographs of intermetallic compounds on Cu side

表 3　B和 C点能谱分析结果 (原子分数, %)

Table 3　EDS analysis results of spots (B and C)

位置	Al	Cu	Zn
B	66.09	31.85	2.07
C	67.31	30.55	2.14

2.4 铝含量对铜铝钎焊接头断口形貌的影响

钎焊接头铜侧断口形貌如图 6所示, Zn-2Al与 Zn-22Al钎焊接头均属于脆性断裂,而 Zn-15Al钎焊接头断口中存在大而浅的韧窝状形貌,如图 6b所示, Zn-15Al钎焊接头发生断裂时,细小均匀分布的 $CuAl_2$相能够阻碍裂纹的扩展, $CuAl_2$相的周围组织

发生塑性变形,需要更大的应力才能使裂纹继续扩展,有利于 Zn-15Al 钎焊接头强度的提高. 从图 6c 中可以看到 Zn-22Al 钎焊接头断裂时粗大的化合物与钎缝剥离时留下的平面形貌, Zn-22Al 钎焊接头由于钎缝内部的 $CuAl_2$ 相尺寸粗大且分布不均匀,在外力作用下,粗大的 $CuAl_2$ 相与周围组织难以实现同步协调变形,在界面处容易产生应力集中而萌生裂纹,成为接头断裂的裂纹源,导致 Zn-22Al 钎焊接头强度降低.

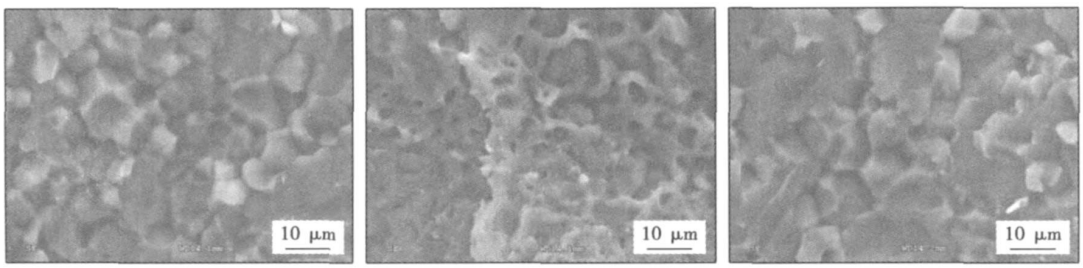

(a) Zn-2Al (b) Zn-15Al (c) Zn-22Al

图 6 钎焊接头铜侧断口形貌

Fig. 6 Fracture micrographs of brazed joint on Cu side

3 结 论

(1) Zn-Al 钎料在铝板上的铺展面积随铝含量的增加呈先增后减趋势,铝含量质量分数为 15% 时,铺展面积最大. 钎料在铜板上的铺展面积随铝含量的升高逐渐增加.

(2)随着铝含量的增加,钎料显微组织逐渐粗化,铝含量质量分数为 22% 时,钎料内部块状组织最为粗大. 钎料中铝含量质量分数为 15% 时,铜铝钎焊接头力学性能最佳,抗剪强度达到 44.04 MPa.

(3)钎料中铝含量较低时,钎缝显微组织主要为锌基固溶体. 当铝含量质量分数增加至 15% 时,钎缝内部出现细小均匀分布的 $CuAl_2$ 相颗粒,对钎焊接头有颗粒强化的作用,继续增加铝含量至 22% 时,钎缝中的 $CuAl_2$ 相变成粗大的条块状,且分布不均匀,易产生应力集中,导致接头力学性能降低.

参考文献:

[1] 薛松柏, 董 健, 吕晓春, 等. LY12 铝合金中温钎焊技术[J]. 焊接学报, 2003, 24(3): 21—24.
Xue Songbai, Dong Jian, Lü Xiaochun, et al. Brazing technology of LY12 Al-alloy at middle temperature[J]. Transactions of the China Welding Institution, 2003, 24(3): 21—24.

[2] 薛松柏, 董 健, 吕晓春, 等. Al/Cu 管异种材料火焰钎焊连接[J]. 焊接, 2003(12): 23—24.
Xue Songbai, Dong Jian, Lü Xiaochun, et al. Flame brazing for dissimilar materials of Al/Cu tube[J]. Welding and Joining, 2003(12): 23—24.

[3] 林三宝, 宋建岭, 杨春利, 等. 铝合金/不锈钢钨极氩弧熔—钎焊接头界面层的微观结构分析[J]. 金属学报, 2009, 45(10): 1211—1216.
Lin Sanbao, Song Jianling, Yang Chunli, et al. Microstructure analysis of interfacial layer with tungsten insert gas welding-brazing joint of aluminum[J]. Acta Metallurgica Sinica, 2009, 45(10): 1211—1216.

[4] Abbasi M, Karimi Taheri B A, Salehi A M T. Growth rate of intermetallic compounds in Al/Cu bimetal produced by cold roll welding process[J]. Journal of Alloys and Compounds, 2001, 319(1—2): 233—241.

[5] Lee W B, Bang K S, Jung S B. Effects of intermetallic compound on the electrical and mechanical properties of friction welded Cu/Al bimetallic joints during annealing[J]. Journal of Alloys and Compounds, 2005, 390(1—2): 212—219.

[6] Ouyang J, Yarrapareddy E, Kovacevic R. Microstructural evolution in the friction stir welded 6061 aluminum alloy (T6-temper condition) to copper[J]. Journal of Materials Processing Technology, 2006, 172(1): 110—112.

[7] Xia C Z, Li Y J, Puchkov U A, et al. Microstructure and phase constitution near the interface of Cu/Al vacuum brazing using Al-Si filler metal[J]. Vacuum, 2008, 82(8): 799—804.

作者简介: 张 满, 男, 1980 年出生, 博士研究生, 讲师. 主要从事新型焊接材料及新工艺方面的研究. 发表论文 8 篇. Email: zhangmansky@163.com

通讯作者: 薛松柏, 男, 教授. Email: xuesb@nuaa.edu.cn

the motion trajectory of welding gun was planned. The 3D model of the welding equipment based on Pro/Engineer working environment was established, the definition of the motion jointing and the parameters of servomotors were set, the virtual prototype motion simulation experiment of the welding equipment was run, the motion trajectory curve was created, and the simulation errors was analyzed. The correctness of modeling the mathematic model was validated, which provided the simulation technology supporting of virtual prototype for developing and manufacturing the welding equipment.

Key words: petroleum drill valve; intersection surface; motion simulation; trajectory curve

Extraction method of welding seam and defect in ray testing image ZHANG Xiaoguang[2], SUN Zheng, HU Xiaolei, HUAN Yuyue (1. College of Mechanical and Electrical Engineering, China University of Mining and Technology, Xuzhou 221116, China; 2. State Key Laboratory of Advanced Welding Production Technology, Harbin Institute of Technology, Harbin 150001, China; 3. Physics & Electronic Engineering Department, Zaozhuang University, Zaozhuang 277160, China). p77—80

Abstract: A practical detection method, which takes advantage of the information contained in the image itself, is presented based on local treatment gradually for attacking the difficulties in accurately detecting and extracting weld seam and defect in ray testing image. First of all, the approximate location of the weld zone in the original image is determined by detecting the regional characteristics of bands; then, the local area where the weld boundaries and defect are in is determined by analyzing gray column waveforms, and the area types are divided into the categories of non-crack and crack class roughly; finally, the detection and extraction of welding defects are realized by using the methods based on Watershed Transform and Beamlet Transform respectively. The results show that the method can accurately detect the weld boundaries and weld defect in various ray images and has good adaptability and practicality.

Key words: ray testing image; welding seam; defect extraction; Watershed Transform; Beamlet Transform

Numerical modeling of welding distortion in thin-walled mild steel pipe DENG Dean, TONG Yangang, ZHOU Zhongyu (College of Materials Science and Engineering, Chongqing University, Chongqing 400045, China). p81—84

Abstract: A thermal-mechanical nonlinear finite element method based on ABAQUS was developed to simulate the temperature, residual stress and strain fields in thin-walled structures welded by arc fusion welding processes. The welding temperature field and the welding distortion in a thin-walled mild steel pipe were predicted by using the developed finite element method. Meanwhile, experiments were carried out to measure the actual welding distortion in the thin-walled pipe welded by an arc-welding robot. The coincidence between the simulation and the experimental results confirmed the validity of the numerical simulation method. The numerical simulation method has established a foundation for prediction of welding distortion in thin-walled structure used in practical engineering.

Key words: finite element method; numerical simulation; welding temperature field; welding distortion

Microstructure and properties of rapidly solidified Ag-Cu-Sn ternary brazing fillers XU Jinfeng, ZHANG Xiaocun, DANG Bo, DAI Weigang (1. School of Material Science and Engineering, Xi'an University and Technology, Xi'an 710048, China; 2. Changshu Shuanghua Electronic Co., Ltd., Changshu 215500, China). p85—88

Abstract: The phase constitution, morphology, electrical resistivity and mechanical properties of $Ag_{42.47}Cu_{57.53-x}Sn_x$ (x= 12.23, 12.94, 13.65, mass fraction, %) prepared by melt-spun method are investigated. The results indicate that the microstructure of the alloys consists of (Ag), α-Cu and a few of $Cu_{13.7}Sn$ phases; with the rise of tin content, the electrical resistivity increases for refining of the microstructure and increasing of grain boundary amount and solute-trapping; on the other hand, fine crystal strengthening and solution hardening will result in the increment of tensile strength from 280 to 360 MPa, but the elongation reduces from 5% to 2.8%. The ranges of solidus and liquidus temperature of those alloys are 590 to 616 ℃ and 615 to 622 ℃ respectively, and the temperature range increases with the increasing of tin content.

Key words: ternary alloy; quenched brazing filler; rapid solidification; microstructure; properties

Dynamic compensation for deformation in laser welding of 3D joint seam GONG Shihua, YU Junfeng, YANG Jianzhong, LI Bin (State Engineering Research Center of Manufacturing Equipment Digitization, Huazhong University of Science and Technology, Wuhan 430074, China). p89—92

Abstract: As there is deformation perturbation in the laser welding process of 3D joint seam, the real-time measurement and dynamic compensation in the welding process is used to track accurately a 3D trajectory. The real-time measuring of the 3D joint seam welding is achieved with a laser visual sensor on a five-axis NC welding machine tool, the bias information of tracking joint seam is transformed from measuring coordinate system to workpiece coordinate system, the feed amount of axes is compensated real time, and the dynamic compensation in the welding process of 3D joint seam is realized. The stability of the loop-closed control system with 3D joint seam measuring feedback is analyzed, and the proposed arithmetic is testified by experiment, which indicates that the real-time measuring and dynamic compensation in the 3D joint seam welding process satisfies the track control requirement in 3D laser welding.

Key words: laser welding; 3D joint seam; dynamic compensation; visual sensor

Effect of $CuAl_2$ phase on properties and microstructure of Cu/Al brazed joint ZHANG Mark[2], XUE Songbai, JI Feng, LOU Yinbin, WANG Shuiqing (1. College of Materials

Science and Technology, Nanjing University of Aeronautics and Astronautics, Nanjing 210016, China; 2. College of Mechanical Engineering, Huaiyin Institute of Technology, Huaian 223001, China; 3. Zhejiang Xinrui Welding Material Co., Ltd., Shengzhou 312000, China). p.93—96

Abstract: Cu/Al dissimilar metals were brazed with Zn-Al filler metals by torch-brazing technology, and the effects of Al on the spreadability and microstructure of Zn-Al filler metal were investigated separately. Moreover, the strength and microstructure of the brazed joint were also studied. Results indicate that the strength of the brazed joints achieves the optimum status when the Al content of filler metals is 15%. SEM and EDS are used to study the microstructure and phase constitution of the filler metals and brazed joints respectively. Experimental results show the microstructures of brazed joints are mainly consisted of Zn-based solid solution when Al content is low. However, $CuAl_2$ intermetallic compounds can form in the brazing seam region with increase of Al content. When Al content is 22 wt%, $CuAl_2$ intermetallic compounds become coarse, and the strength of brazed joint decreases.

Key words: Cu/Al brazed joint; mechanical property; microstructure; $CuAl_2$ phase

FEM simulation of calibration on strain release coefficients in blind hole method MA Wenbo[1,2], CHEN Shuguang, LI U Huijiong, LI N Wen, SHEN Yulong, LIU Jipu (1. School of Mechanical Engineering, Xiangtan University, Xiangtan 411105, China; 2. Hunan Special Equipment Inspection & Testing Center, Changsha 410000, China). p.97—100

Abstract: The significant error of the measuring result may arise when measuring welding residual stress by means of the blind hole method. Because the stress around the hole exceed the yield limit, the plastic deformation induces plastic strain. Therefore, based on the principle of the calibration experiment, the strain release coefficients A and B of the steel Q345R are determined. According to the energy parameter S, the strain release coefficient A and B can be revised by the variation formulas by this method, the result of measuring high residual stress can be more accurate. Based on the strength theory, the strain release coefficients A and B of steel Q345R, which were numerically calculated by the finite element method (FEM), coincide well with the calibration experiment results. So the FEM determination of the strain release coefficients A and B is viable.

Key words: blind-hole method; welding residual stress; strain release coefficient; calibration experiment; finite element method

Effects of CO_2 laser beam action on temperature of TIG arc WU Shikai, XIAO Rongshi (Institute of Laser Engineering, Beijing University of Technology, Beijing 100124, China). p.101—104

Abstract: In order to understand the effects of a vertically incident CO_2 laser beam on the tungsten-inert gas (TIG) arc characteristics, the spectra of the arc plasma with the action of a vertically incident laser beam are analyzed. The electron temperature of the arc plasma is calculated by the boltzmann plot method. The results show that the electron temperature of the arc plasma with the action of CO_2 laser beam radiation is increased between the laser acting position and anode zone. The influences of laser power, arc current and laser acted position on electron temperature are also studied. The charges in electron temperature indicate that the inverse bremsstrahlung absorption of laser energy is the dominant factor influencing the electron temperature of TIG arc plasma with the action of CO_2 laser beam.

Key words: CO_2 laser; TIG arc; spectral diagnosis; electron temperature; inverse bremsstrahlung absorption

Joint performance of duplex stainless steel 2205 by laser-MIG hybrid welding WANG Zhiyu, XU Haigang, WU Weiwei, ZHANG Lijuan[2] (1. Research and Development Center, Baoshan Iron & Steel Co., Ltd., Shanghai 201900, China; 2. TWI, Cambridge CB21 6AL, UK). p.105—108

Abstract: Phase ratio in weld metal and heat affected zone of duplex stainless steel will be unbalanced and joint properties deteriorated because of fast cooling rate after welding by conventional high energy density beam, so the duplex stainless steel 2205 is welded by using laser-MIG hybrid welding method and the microstructure, mechanical property and corrosive property of welded joint are analyzed. The results show that the phase ratio of ferrite in weld metal and heat-affected zone is controlled between 40% —70%, the microhardness and tensile strength of the joint are higher than those of base metal, the impact toughness of weld metal, fusion line and heat-affected zone at —40 ℃ is 73, 205, 190 J/cm² respectively and the critical pitting temperature (CPT) of weld bead is 49 ℃, near the same as that of base metal. So the good joint performance of duplex stainless steel 2205 can be obtained by laser-MIG hybrid welding.

Key words: duplex stainless steel; hybrid welding; microstructure; mechanical property; critical pitting temperature

Microstructures and corrosion-resistant performance of Al twin wire MIG welded joint RUAN Ye, QIU Xiaoming, GONG Wenbiao[2], ZHAO Shihang, SUN Daqian[2] (1. School of Materials Science and Engineering, Jilin University, Changchun 130025, China; 2. School of Materials Science and Engineering, Changchun University of Technology, Changchun 130012, China). p.109—112

Abstract: Microstructures and corrosion-resistant performance of 6082-T6 Al twin wire MIG welded joint are studied by SEM and XRD technology. Experiments show that the welded seam is composed of a lot of α-Al, α-Al+ Mg_2Si and a few Mg_2Si, moreover, Mg_2Si largely presents in the grain boundary. Corrosion-resistant performance is studied by measuring the potentiodynamic polarization curves and corrosion surface morphologies of twin wire MIG welded joint, and the results show that corrosion-resistant performance of the matrix is better than that of the weld seam, and precipitated Mg_2Si decreases the corrosion-resistant performance of the weld seam.

Key words: 6082-T6 Al alloy; twin wire MIG; microstructures; corrosion